Algorithms and Models for Cellular Based Topography Simulation

Ernst Strasser, *Student Member, IEEE,* and Siegfried Selberherr, *Fellow, IEEE*

Abstract—**A general simulation method for three-dimensional surface advancement has been developed and coupled with physical models for etching and deposition. The surface advancement algorithm is based on morphological operations derived from image processing which are performed on a cellular material representation. This method allows arbitrary changes of the actual geometry according to a precalculated etch or deposition rate distribution and can support very complex structures with tunnels or regions of material which are completely disconnected from other regions. Surface loops which result from a growing or etching surface intersecting with itself are inherently avoided. The etch or deposition rate distribution along the exposed surface is obtained from macroscopic point advancement models which consider information about flux distributions and surface reactions of directly and indirectly incident particles.**

I. Introduction

TOPOGRAPHY simulation assists in understanding the time evolution of topographical features in advanced device structures. As the device dimensions are reduced further, three-dimensional models and algorithms are increasingly necessary for wafer topography evaluation. The numerical methods and algorithms applied for the movement of the actual surface play a key role in topography simulation because they lead to differences in accuracy, robustness, and efficiency of the simulation tools.

In recent years a variety of surface evolution algorithms has been studied to build three-dimensional topography simulators. Among them many algorithms have been reported for resist development in lithography simulation [1]–[7], only a few methods have been proposed for the simulation of etching and deposition processes [8]–[11]. Basically there are two types of algorithms used for three-dimensional topography simulation. Volume-removal methods divide the material being etched into a large array of rectangular prismatic cells. Each cell is characterized as etched, unetched, or partially etched. During etching cells are removed one by one according to the local etch rate and the number of cell faces exposed to the etching medium. These algorithms have been successfully used in three-dimensional lithography simulation [2]–[4]. Volume-removal methods can easily handle arbitrary geometries, but unfortunately they suffer from inherent inaccuracy, because they favor certain etch directions as was found by many researchers [2], [4], [12]. Therefore it is difficult to apply these algorithms for general etching and deposition problems. The second type of surface evolution algorithms represent the surface of the material being etched by using a mesh of points which are connected by line segments to form triangular facets [8], [12]. Depending on the implementation, either the mesh points or the facets are moved according to the local etch rates. A mesh management is necessary to maintain the mesh as it moves in time. In general, these algorithms deliver highly accurate results, though with potential topological instabilities such as erroneous surface loops which result from a growing or etching surface intersecting with itself. The surface loops must be located and removed to conserve memory and maintain efficiency of the simulation tool [13].

In this paper we present a general method for surface evolution in topography simulation which inherently avoids the formation of unphysical surface loops. This method is based on fundamental morphological operations derived from image processing which are performed on a cellular material structure. In Section II we first develop the algorithm for surface movement starting from some basic morphological operations. In Section III we then couple the surface advancement algorithm with macroscopic process models for plasma etching and thin film deposition. Finally, in Section IV, several simulation results of etching and deposition processes are presented which demonstrate the applicability of our method to a wide range of problems in topography simulation.

II. A General Algorithm for Surface Advancement

The algorithm for surface advancement is based on morphological operations which provide a well defined method for altering a given image with respect to some predetermined geometric shape known as *structuring element* [14].

For our application two basic operations are of special importance: *Minkowski subtraction* and *Minkowski addition.*

Given two images A and B, the Minkowski subtraction $A \ominus B$ has the effect of "shrinking" the image A in a manner determined by B as shown in Fig. 1(a). This operation is also called *erosion* operation. In contrast, the Minkowski addition $A \oplus B$ has the effect of "expanding" the image A in a way determined by B as shown in Fig. 1(b). This operation is also known as *dilation* operation. Associated with the operations erosion and dilation the image B is called structuring element.

The result of the Minkowski operations can be obtained simply by moving the structuring element along the boundary of the image A and searching for the inner and outer contour of the area which is covered during the movement. An exact

Manuscript received June 9, 1994; revised January 31, 1995. This work was supported by Digital Equipment Corporation, Hudson, MA, and Siemens Corporation, Munich, Germany. This paper was recommended by Associate Editor S. G. Duvall.

The authors are with the Institute for Microelectronics, Technical University of Vienna, A-1040 Vienna, Austria.

IEEE Log Number 9413231.

0278-0070/95$04.00 © 1995 IEEE

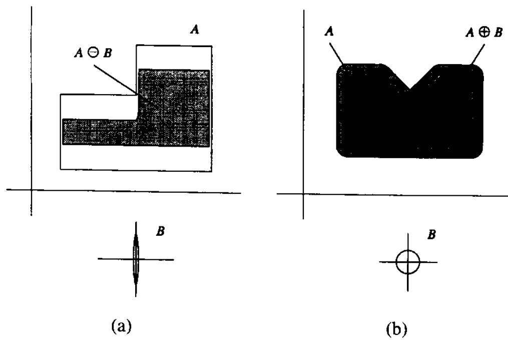

Fig. 1. Basic morphological operations. (a) Erosion as shrinking. (b) Dilation as expanding.

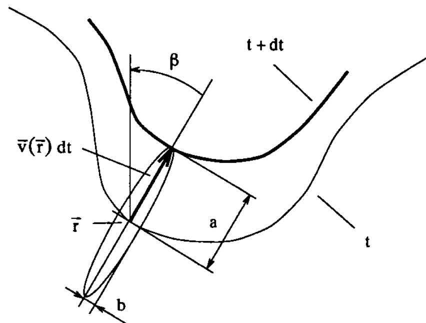

Fig. 2. The structuring element for anisotropic surface advancement.

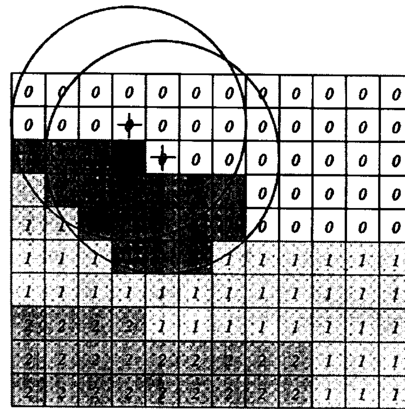

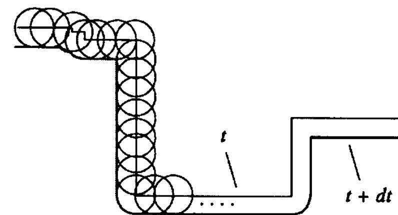

Fig. 3. The material representation. The considered surface cell is dark shaded, the number in the cell denotes the material identifier.

mathematical description of the morphological operations is given in [14].

As during topography simulation the surface moves in time, the initial geometry also either decreases or increases depending on the performed process. If we consider the simulation geometry as a black and white image (material and vacuum), etching of material can be described using the erosion operation, whereas deposition processes can be simulated by means of the dilation operation [15], [16]. The way how the surface evolves at a certain time step is predetermined by the spatial dimensions of the employed structuring element. Until now, the shape of the structuring element was constant along the surface boundary. However, in general, the etch or deposition rates vary along the exposed surface because they depend on local surface conditions. Therefore the spatial dimensions of the structuring element are determined by the local etch or deposition rate multiplied by the time step. Usually, for anisotropic two-dimensional simulation, the structuring element is an ellipse with constant ratio of major to minor axis which is applied in the direction of the local etch or deposition rate vector as shown in Fig. 2, for isotropic movement of the surface point the applied structuring element changes into a circle.

The material is represented using an array of square or cubic cells, where each cell is characterized as etched or unetched. Additionally, a material identifier is defined for each cell; therefore, material boundaries need not be explicitly described as shown in Fig. 3. One cell is represented by eight bits, where one bit is used as an etch flag, the remaining seven bits allow to describe 128 different materials in the simulation region. The surface boundary consists of unetched cells that are in contact with fully etched cells. Cells on the surface are exposed to the etching medium or to the deposition source, and etching or deposition proceeds on this surface. A linked surface cell list stores dynamically array addresses and rate information of exposed material cells. To advance the surface a structuring element whose spatial dimensions are related to the local etch or deposition rate is applied for the exposed cells. Depending on the simulated process either material cells are removed or added which are located within the structuring element.

In case of deposition the structuring element is centered at the midpoint of the considered surface cell, whereas in case of etching the structuring element is applied at the midpoints of neighbored cells which are located adjacent to the exposed cell sides of the surface cell. The reason why different points of attachment are chosen is explained in Fig. 4. As the midpoint of a cell is considered to decide if a cell is located inside or outside of a structuring element, the structuring element must be applied at the neighbored cell in case of etching to advance the surface correctly. Assume an etch radius (etch rate multiplied by the time step) of two cell sides. Only for the shown point of attachment in Fig. 4(a) exactly two cells are removed in vertical direction. In case of deposition the midpoint of the considered surface cell has to be chosen as center of the structuring element as shown in Fig. 4(b) to move the surface the correct distance.

The idea to take more than one cell into consideration during one time step in cell based simulations was first introduced

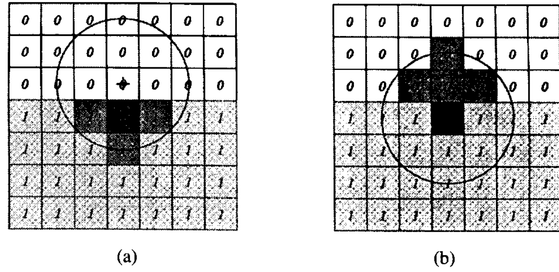

Fig. 4. The point of attachment of the structuring element in case of (a) etching and (b) deposition.

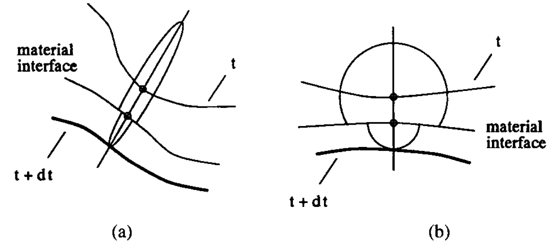

Fig. 5. Special treatment of material boundaries. (a) Anisotropic and (b) isotropic movement of surface points.

by Toh [12]. He proposed to use the Huygens principle to remove cells during isotropic etching which leads to a similar algorithm for this process type. The algorithm described in this paper provides general surface movement using different shapes of structuring elements. Usually, for anisotropic three-dimensional surface advancement structuring elements are ellipsoids, for isotropic movement of surface points structuring elements are spheres, although there is no restriction on the shape of the applied structuring elements. In order to keep the simulation geometry unchanged during one time step only the etch flag is modified by the structuring element. When all the morphological operations are performed, the material indices of marked cells are set to the corresponding material which actually changes the simulation geometry. In case of etching the material index of a marked cell is set to zero to describe a vacuum cell, in case of deposition the material index changes into the index of the deposited material. After each time step, the exposed boundary has to be determined. Therefore all cells of the material array are scanned. Material cells are surface cells if at least one cell side is in contact with a vacuum cell. The exposed sides of the detected surface cells finally describe the material surface at a certain time step.

In case of etching it is important that the etch front at material boundaries evolves correctly, since interfaces between different materials in general lead to an abrupt change in etch rates. Therefore a structuring element is only allowed to remove a cell whose cell index is equal to the index of the exposed cell although the midpoint of the considered cell may be located within the structuring element. If a structuring element extends over a material boundary a second morphological operation must be performed at the interface cell as shown in Fig. 5. The etch rate for this second operation is calculated regarding the etch rates on both sides of the material interface and depending on how far the structuring element reaches into the other material.

The surface advancement algorithm described in this paper is physical correct and robust. However, the accuracy of the simulation method is sensitive to discretization.

The approximation of circles with square cells leads to faceting. The caused discretization error can propagate such that the final profile will be multifaceted. An expected circular profile (e.g., during isotropic etching from a single point source) will look more like a polygon. This effect is discussed in Fig. 6. The etch rate for this example is 1.0 μm/s and the time step is 0.1 s. Fig. 6(a) and (b) show simulation results for a different number of used cells. In Fig. 6(a) the cell density is 100 cells per micrometer, therefore the etch radius is 10 cells per time step. In Fig. 6(b) the cell density is increased to 300 cells per micrometer for an etch radius of 30 cells per micrometer. Both profiles show reasonable circular profiles, although facets are formed. However, in contrast to the original cell-removal algorithm (Fig. 6(c)), the discretization error decreases with greater cell density. Therefore a typical radius of a structuring element should contain at least 10 cells per time step. Fig. 6(d) shows the comparison with the nearly perfect circular profiles of the string-algorithm.

The second type of discretization error occurs when the cell size is large compared to the size of the structuring element. A cell is represented as etched or unetched, it does not keep track of the area that has been etched. In cases where the etch radius becomes smaller than the cell size the etch front will not move because etching does not accumulate. This discretization error is discussed in Fig. 7. The etch rate for this example is given by

$$v(x,\, z)_{[\mu\mathrm{m/s}]} = 2|x_{[\mu\mathrm{m}]}| + 0.06, \tag{1}$$

the time step is 0.1 s. Fig. 7(a) and (b) show simulation results for a different number of used cells. In Fig. 7(a) 100 cells per micrometer are used, so the etch radius at the edges $|x| = 0.5$ μm is 10.6 cells per time step and at $x = 0\,\mu$m it is 0.6 cells per time step. Therefore the cell at $x = 0\,\mu$m will not be etched and the etch front at this region will not move. To handle this, the cell size must be at least smaller than the weakest etch radius. This is the case in Fig. 7(b) where 300 cells per micrometer are used. In areas where the etch front moves, a position error may occur due to the accumulation of the discretization error. However, by increasing the cell density this problem can be reduced (compare Fig. 7(a) and (b)). Using 300 cells per micrometer (Fig. 7(b)) the simulation shows very good agreement with the corresponding simulations made with the original cell-removal algorithm (Fig. 7(c)) and the string algorithm (Fig. 7(d)).

In order to retain accuracy, the time step during the simulation is controlled in such a way that the etch rate of all exposed cells is averaged and for the resulting rate an etch radius of typically 15 cells is chosen. The computation time of a simulated time step is therefore directly proportional to the number of boundary cells. In two dimensions the computation time goes roughly as $O(N^2)$ (where N is the number of cells in one dimension), because also the number of simulated time

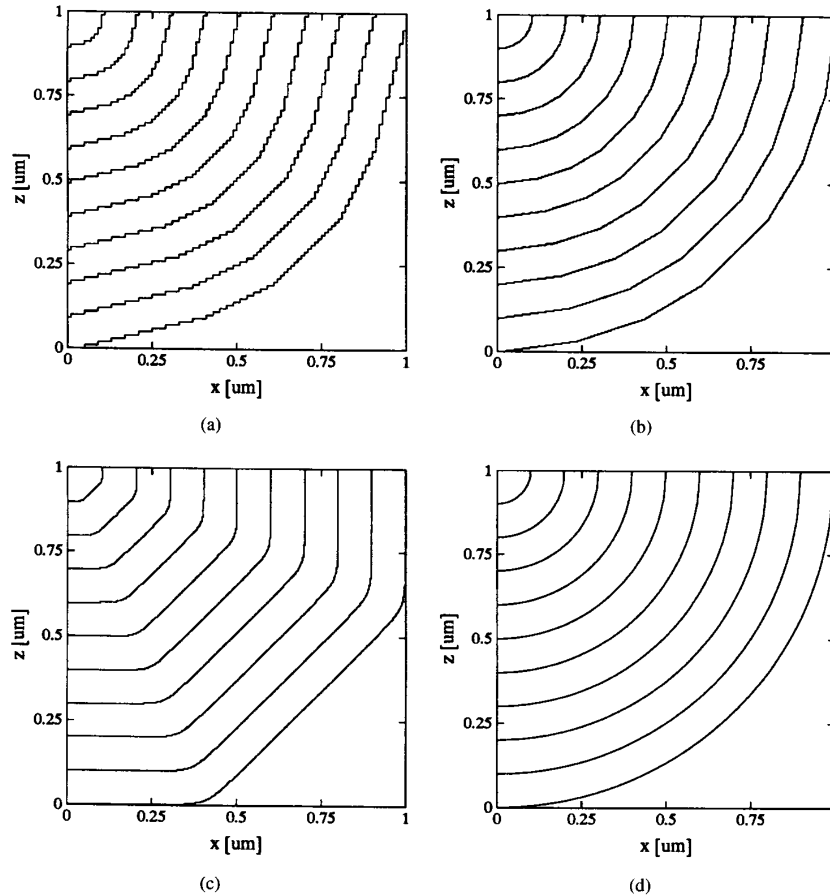

Fig. 6. Faceting during uniform circular etching. (a) 100 cells per micrometer. (b) 300 cells per micrometer. (c) Original cell-removal algorithm. (d) String algorithm.

TABLE I
COMPUTATION TIMES IN SECONDS FOR THE ETCH SIMULATION IN FIG. 7 MEASURED ON AN HP 9000/755 WORKSTATION

Number of used cells	Structuring Element Algorithm	Cell-Removal Algorithm	String Algorithm
100 × 100	1.2	48.1	
200 × 200	5.3	532.4	1.3
300 × 300	12.7	1529.2	

steps grows linearly with the number of cells. The computation times for the etch simulation in Fig. 7 are shown in Table I.

In three dimensions the algorithm run time is $O(N^3)$, because the number of boundary cells goes as $O(N^2)$. Therefore the algorithm is more efficient than the original cell-removal method where the computation time in two-dimensions goes as $O(N^3)$ and in three dimensions even as $O(N^5)$.

III. Modeling of Etching and Deposition Processes

Many topography processes are affected by the shape of the surface. Successful two-dimensional simulation programs for etching and deposition processes use macroscopic point advancement models that consider information about particle fluxes and surface reactions to calculate etch or deposition rate distributions along the exposed surface [17]–[21]. This approach has also been used in SAMPLE-3D [22] with great success, despite the difficulty of maintaining a surface mesh and avoiding erroneous surface loops. The application of macroscopic point advancement models is extremely desirable, since a variety of process models for etching and deposition in the literature already exists and quantities such as etch or deposition rates are easily measurable in semiconductor technology.

To determine the rate contributions of incoming particles both in etching and deposition the simulator must be capable to calculate the resulting particle flux incident at a surface point. Therefore a spherical coordinate system with polar angle ϑ and azimuth angle φ is assumed and the region above the wafer is divided up into several surface patches ($N_\varphi \times N_\vartheta$) as shown in Fig. 8. The incident flux is then integrated over those patches of the hemisphere which are visible from the surface point $\vec{r}$. To determine if a surface patch is visible from a point on the surface a shadow test has to be performed along a given direction which is within the cellular structure simply the matter of following a discretized line of cells from the surface cell to the boundary of the simulation area. If any cell on this

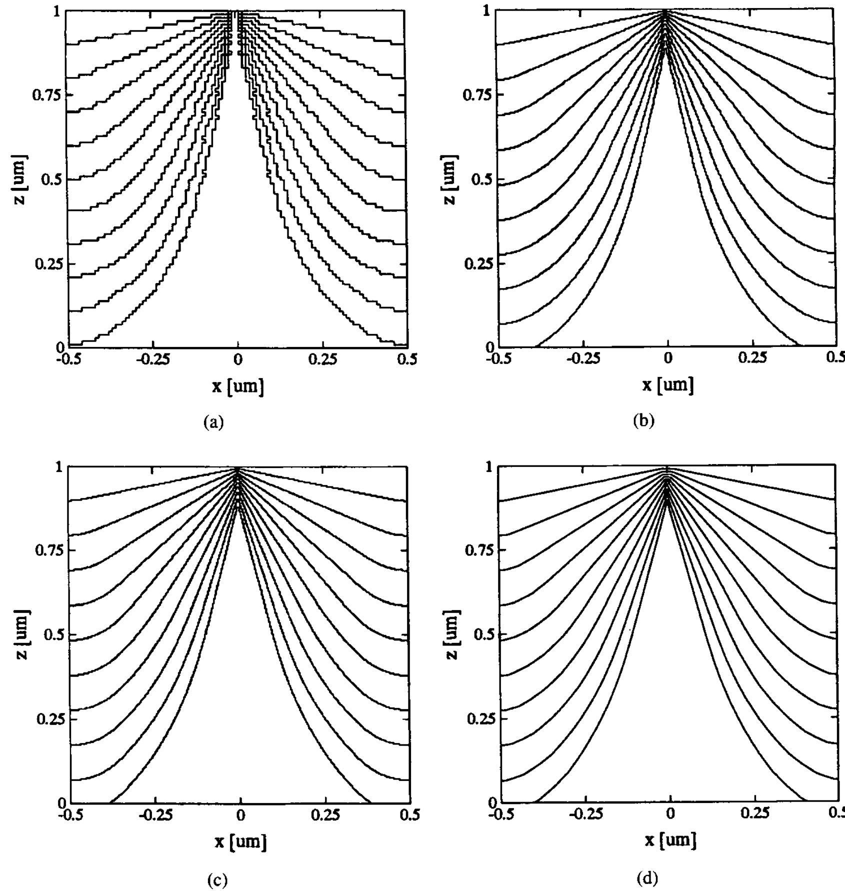

Fig. 7. Position error due to discretization using a triangular etch rate function. (a) 100 cells per micrometer. (b) 300 cells per micrometer. (c) Original cell-removal algorithm. (d) String algorithm.

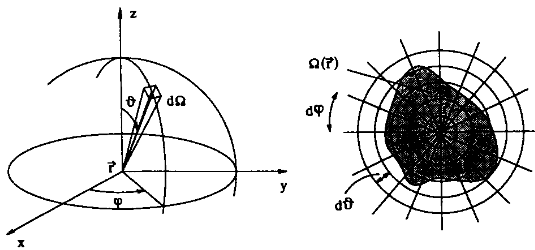

Fig. 8. The calculation of the incident particle flux.

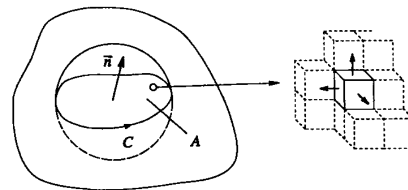

Fig. 9. .The calculation of the local surface orientation.

line is a material cell, then the surface cell is shadowed. The calculation of the visible solid angle $\Omega = \Omega(\vartheta, \varphi)$ with $d\,\Omega = \sin\varphi\, d\varphi\, d\vartheta$ (the radius of the hemisphere may be normalized to one) is then reduced to a series of shadow tests. The number of shadow tests required at a surface point corresponds to the number of patches of the hemisphere. As this number is a constant (typically 90×45 ($N_\varphi \times N_\vartheta$) patches are used), the time required to calculate the visible solid angle for the entire surface is proportional to the number of surface points.

Some processes such as ion milling or crystal etching show a strong dependence on the local surface orientation. The cellular material representation does not provide this information inherently, but the calculation is rather simple. At each exposed side of a surface cell a normal vector can be defined as shown in Fig. 9. The surface normal at a given surface point is then calculated by summing up the normal vectors of surface cells within a certain vicinity to that surface point. For practical simulations surface cells that are located within a sphere are considered, a sphere radius of typically 10–15 cells provides highly accurate results.

Etch Models: As a basic concept we consider a linear combination of isotropic and anisotropic reactions of directly and indirectly incident particles to calculate the resulting velocity vector of a surface point. A similar concept was

first implemented by Tazawa *et al.* [21] for two-dimensional modeling of etching processes coupled with a string based algorithm for surface movement. The isotropic reaction is mainly a chemical reaction affected by a reactive gas, in which the reactive particles have short mean free paths and move randomly. The anisotropic reaction is a physical or chemical reaction, where the particles have long mean free paths compared to the device dimensions and angular particle fluxes must be taken into account. The following etch rate components contribute to the resulting velocity of a surface point:

1) *Isotropic Etching:* A chemical reaction caused by reactive particles of a plasma, whose mean free paths are short compared to characteristic device dimensions, results in an isotropic movement of the surface. The particles are moving randomly and no momentum transfer to the surface takes place. The etch rate has no orientation or flux dependencies and is described as a constant:

$$v_{iso}(\vec{r}) = R_{iso}. \tag{2}$$

2) *Directly Incident Ions:* In reactive ion etching and ion milling high energetic ions which are accelerated by the electric field cause etching by physical sputtering. The etch rate at a surface point must be correlated to a sputter yield curve $S(\alpha)$, which has typically been described as a cosine power series [17]. The particle flux $F_i(\Omega)$ of incident ions may be described by a Gaussian distribution with the standard deviation σ as fitting parameter [8] or simply as a delta function along a given direction [19]. The etch rate along the surface normal is expressed as

$$v_i(\vec{r}) = R_i \int_\Omega F_i(\Omega)\, S(\alpha)\, \cos\alpha \, \mathrm{d}\Omega \tag{3}$$

$$F_i(\Omega) = \exp(-\vartheta^2/2\,\sigma^2)/N, \tag{4}$$

$$S(\alpha) = \sum_{n=1}^{m} a_n \cos^n \alpha, \tag{5}$$

where α is the angle of incidence with respect to the surface normal and N is a normalizing factor of the incident flux so that R_i is the etch rate on a flat substrate without shadowing.

3) *Directly Incident Neutrals:* Neutral particles cause etching mainly by a chemical reaction. The particles are assumed to arrive with mean free paths which are large compared to characteristic device dimensions. The flux distribution of incoming particles $F_n(\Omega)$ can be described by a hypercosine function [19]. Neutral particles do not exhibit a sharp peak in their flux distribution because they are not affected by the electric field. The etch rate along the surface normal is characterized as

$$v_n(\vec{r}) = R_n \int_\Omega F_n(\Omega)\, \cos\alpha \, \mathrm{d}\Omega, \tag{6}$$

$$F_n(\Omega) = \cos^m(\vartheta)/N, \tag{7}$$

where R_n is the etch rate of directly incident neutrals on a flat wafer without shadowing. The chemical etch rate of neutral particles may be enhanced by the presence of directly incident ions that damage the surface. A model to incorporate this effect was given by Scheckler and Neureuther [8],

$$R_{n,i} = R_n \left[1 + D_i \int_\Omega F_i(\Omega)\, \mathrm{d}\Omega\right], \tag{8}$$

where R_n denotes the etch rate due to neutrals without the presence of ions and D_i is a damage parameter that relates the particle flux of directly incident ions to the enhancement of the chemical etch rate.

4) *Reflected Particles:* A simple model to consider reflected particles was proposed by Tazawa *et al.* [19]. Indirectly incident particles are assumed to arrive uniformly from all directions above the wafer plane to which the plasma is not visible. The etch rate along the surface normal is expressed as

$$v_r(\vec{r}) = R_r \int_{H-\Omega} \cos\alpha \, \mathrm{d}\Omega, \tag{9}$$

where H is the entire hemisphere and R_r relates the particle flux to the actual etch rate.

The linear combination of the etch rate components described above leads to

$$v_{iso}(\vec{r}) = R_{iso}, \tag{10}$$

$$\begin{aligned} v_{dir}(\vec{r}) = {} & R_i \int_\Omega F_i(\Omega)\, S_i(\alpha)\, \cos\alpha \, \mathrm{d}\Omega \\ & + R_n \left[1 + D_i \int_\Omega F_i(\Omega)\, \mathrm{d}\Omega\right] \int_\Omega F_n(\Omega)\, \cos\alpha\, \mathrm{d}\Omega \\ & + R_r \int_{H-\Omega} \cos\alpha \, \mathrm{d}\Omega. \end{aligned} \tag{11}$$

To advance the surface subsequently a spherical and an ellipsoidal structuring element are applied. The radius of the spherical element is determined by the isotropic rate (10) multiplied by the time step. The ellipsoidal structuring element is applied in the direction of the anisotropic etch rate vector. The major axis of this element is calculated by multiplying the anisotropic rate (11) with the time step, the length of the minor axes are chosen in such a way that the ratio of major to minor axis becomes constant (e.g., 5).

Deposition Models: Deposition modeling is based on the original work of Blech who developed a model for describing two-dimensional profiles of evaporated thin films over steps [23]. This model is directly applicable to three-dimensional simulation. In three dimensions the components of the growth vector can be calculated by

$$v_x(\vec{r}) = R_d \int_\Omega F_d(\Omega)\, \cos\varphi\, \sin\vartheta \, \mathrm{d}\Omega, \tag{12}$$

$$v_y(\vec{r}) = R_d \int_\Omega F_d(\Omega)\, \sin\varphi\, \sin\vartheta \, \mathrm{d}\Omega, \tag{13}$$

$$v_z(\vec{r}) = R_d \int_\Omega F_d(\Omega)\, \cos\vartheta \, \mathrm{d}\Omega, \tag{14}$$

where R_d denotes the deposition rate on a flat wafer without shadowing and $F_d(\Omega)$ is the angular flux distribution function of incoming particles. Different assumptions on the

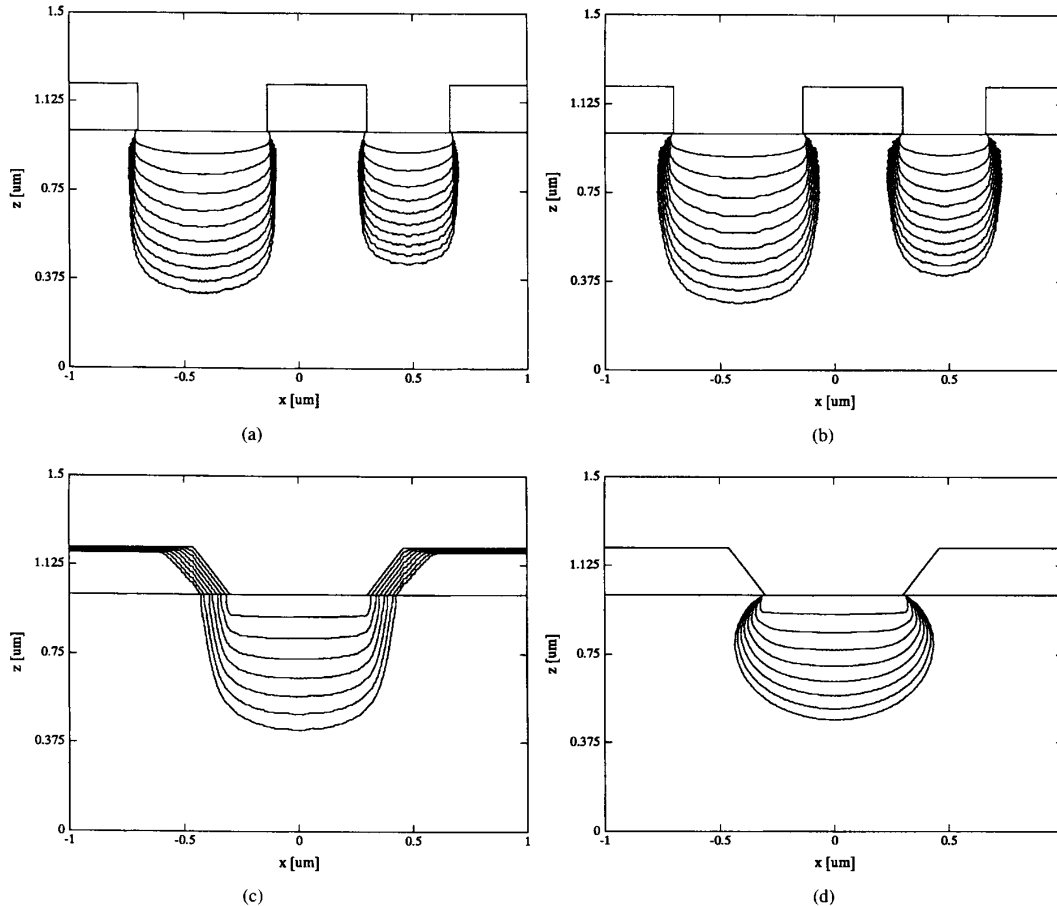

Fig. 10. Plasma etching of trenches varying several model parameters. (a) Aperture effect due to different mask size openings. (b) Result with addition of particle reflection. (c) Reactive ion etching including physical sputtering. (d) Neutral etching only.

flux distribution function result in evaporation or sputter deposition processes. Original work on sputter deposition processes assumed the incident particles to arrive equally from all directions [23], subsequent work showed a cosine dependence on ϑ [24]. A general cosine-based flux distribution function may be expressed as [8]

$$F_d(\Omega) = \cos^n(A\vartheta)/N, \quad \text{for}\,\vartheta \leq \pi/2A\,\text{otherwise}\,0. \tag{15}$$

The parameter A restricts the angle of incoming particles, the parameter n allows over-cosine and under-cosine distributions. After calculating the growth vector for exposed cells the surface is advanced in the same way as described above for the directional etch rate component.

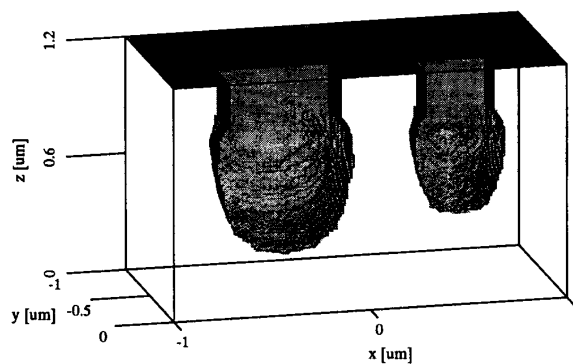

Fig. 11. Ion enhanced plasma etching of trenches showing the barreling phenomenon and the aperture effect.

IV. Simulation Results

Several simulation results presented below demonstrate the robustness and flexibility of the simulation method. The examples in Fig. 10 show two-dimensional plasma etch simulations of trenches varying several model parameters. Fig. 10(a) shows the typical barreling phenomenon which results in ion enhanced plasma etching due to high energetic ions that increase the etch rate where they hit the surface (mainly at the bottom of the trench) and due to reactive neutrals which also attack the sidewalls. The picture also shows the well known aperture effect (etch rate decreasing due to limited delivery of ions and radicals) resulting in a deeper trench where the

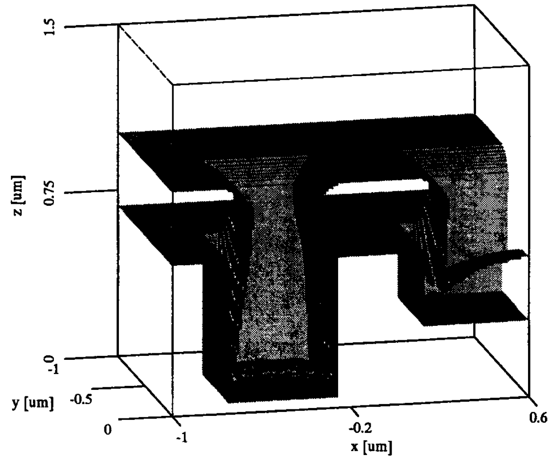

(a)

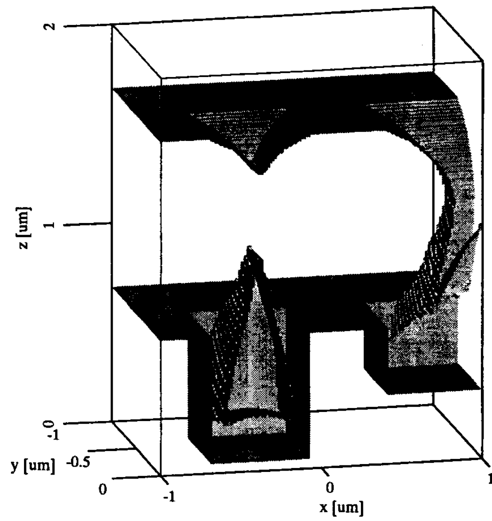

(b)

Fig. 12. Sputter deposition simulation showing the formation of a vacuum hole. (a) 400 s deposition time. (b) 1200 s deposition time.

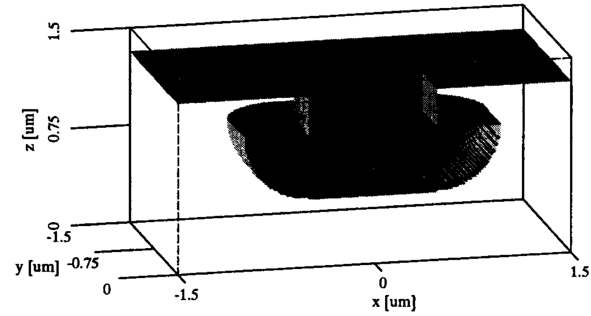

(a)

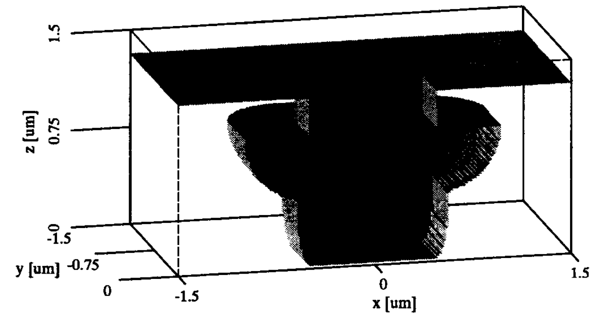

(b)

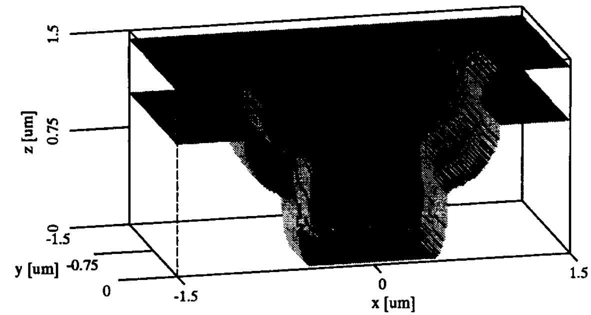

(c)

Fig. 13. Patterning and metallization of a contact hole. (a) Isotropic etching step. (b) Directional etching step. (c) Sputter deposition.

mask size opening is larger. The chemical etch rate for this example was $R_n = 0.65$ nm/s with $D_i = 6.0$ (see (8)) and the etch time was 400 s. The parameter of the particle distribution functions were $\sigma = 2.0$ and $m = 1.0$ (see (4) and (7)). Fig. 10(b) shows the result when reflection of particles with $R_r = 0.15$ nm/s is considered. The anisotropy of the trench becomes worse due to additional side wall etching. Fig. 10(c) shows reactive ion etching where the physical sputtering effect predominated and also the mask was eroded. The etch rates of the mask and of the substrate were $R_i = 0.07$ nm/s and $R_i = 0.65$ nm/s, respectively, and the sputter yield function was $S(\alpha) = 3.27 \cos\alpha + 13.11 \cos^2\alpha - 15.38 \cos^4\alpha$ (see (5)) [25]. Fig. 10(d) shows etching caused by reactive neutrals only leading to a relatively poor anisotropy of the trench. The etch rate of the substrate was $R_n = 0.65$ nm/s, the mask was not etched, and the simulation time here was 1000 s. All the simulations were performed using 300 cells per micrometer for the geometry representation, the required simulation time varied from 30–90 s.

Fig. 11 shows three-dimensional simulation of ion enhanced plasma etching of trenches. We took almost the same model parameters as for the example depicted in Fig. 10(a). Only the standard deviation σ of the ion distribution function (4) was changed into 5.0 which led to an enhanced barreling effect of the trench. Again, the aperture effect due to different mask size openings is visible. The simulation was performed using 90 cells per micrometer for the material array and took 27 minutes of simulation time.

Fig. 12 shows a sputter deposition simulation using a cosine based flux distribution function. Fig. 12(a) depicts the simulation result after 400 s deposition time. The growth rate of the

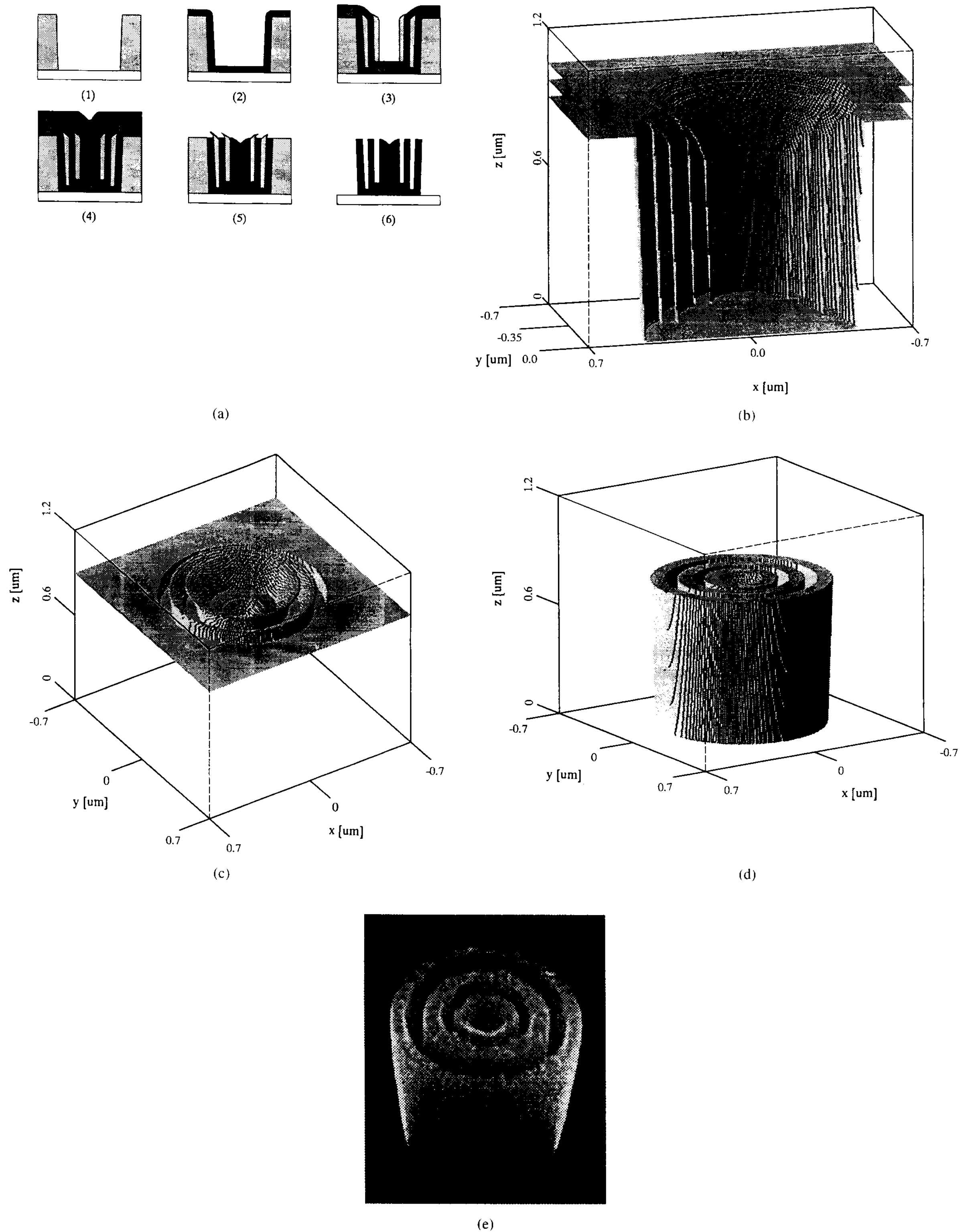

Fig. 14. Simulation of the fabrication process of a stacked capacitor cell. (a) Process sequence of capacitor cell structure. (b) Simulation result after second oxide spacer formation. (c) Simulation result after etch back the polysilicon layer. (d) Final cell structure. (e) SEM photograph of original cell structure.

deposited film at each point strongly depends on the surface topology because of shadowing. The deposition rate for this example was $R_d = 0.85$ nm/s, the parameters of the particle distribution function were $A = 1.0$ and $n = 1.0$ (see (15)). Fig. 12(b) shows the simulation result when the deposition time was increased to 1200 s. The deposited film growths together and therefore a vacuum hole is formed. As points at the inner surface are completely shadowed the surface will not move further at this region and the formed hole will be visible at any later simulation time. The simulation was performed using 90 cells per micrometer for the material representation and took 47 minutes of simulation time.

Simulation results for patterning and metallization of a contact hole are shown in Fig. 13. The simulation began with a wet etching step that etched the substrate isotropically to a depth of 0.5 μm as shown in Fig. 13(a). The etch rate for this etching step was $R_{iso} = 0.5$ nm/s and the simulation time was 1000 s. Subsequently, simple directional etching with an etch rate of $R_{dir} = 0.5$ nm/s and a simulation time of 1000 s was performed for 0.5 μm additional material removal. Fig. 13(b) shows the simulation result after this second etching step. As a next simulation step the mask was removed with wet etching and a sputter deposition simulation with a deposition rate of $R_d = 0.85$ nm/s and a deposition time of 500 s took place. The parameters of the particle distribution function were $A = 1.0$ and $n = 1.0$ (see (15)) which led to an acceptable step coverage of the deposited film as shown in Fig. 13(c). 60 cells per micrometer were used for the geometry representation, the whole fabrication of the contact hole took 53 min of simulation time.

The fabrication process of a stacked capacitor cell structure was simulated in Fig. 14. Fig. 14(a) illustrates the process sequence of the capacitor cell structure. Several layers of polysilicon separated by oxide spacers serve to enlarge the area of the capacitor cell which was proposed by Temmler for high density dynamic RAM's [26]. Fig. 14(b) shows the simulated cell structure after the second oxide spacer formation. The simulation began with a planar oxide layer. First the storage node is patterned using a circular mask. The etching process is modeled by using a combination of isotropic and directional etch rates. The etch rates for this simulation step were $R_{iso} = 0.05$ nm/s and $R_{dir} = 0.65$ nm/s, the etch time was 1400 s. Next, isotropic deposition of a polysilicon layer was performed with $R_{iso} = 0.5$ nm/s and 160 s deposition time. This was followed by an isotropic deposition of a oxide layer with $R_{iso} = 0.2$ nm/s and a deposition time of 400 s. The oxide is then etched back 120 s with simple directional etching to form the first oxide spacer. Isotropic deposition of polysilicon and the two process steps to form the oxide spacer are then repeated to obtain the simulation result shown in Fig. 14(b). Next, the cell structure is filled up with polysilicon ($R_{iso} = 0.5$ nm/s, deposition time 1000 s) and subsequently etched back 1300 s with an etch rate of $R_{dir} = 0.6$ nm/s. Fig. 14(c) shows the cell structure after this simulation step. Finally, the whole oxide was removed by wet etching with $R_{iso} = 0.3$ nm/s and 2500 s simulation time. The final simulated cell structure is shown in Fig. 14(d). Fig. 14(e) shows a SEM photograph of the original capacitor cell structure. 120 cells per micrometer were used for geometry representation, the whole simulation took 102 minutes of calculation time. All examples in this paper were simulated on an HP 9000/755 workstation.

V. Conclusion

A method for general surface advancement in topography simulation was presented which is based on fundamental morphological operations derived from image processing. The basic idea behind this method is to apply a structuring element along the exposed surface which in case of etching removes material cells from a underlying cellular structure. The surface evolution depends on precalculated etch or deposition rate distributions which are obtained from conventional macroscopic point advancement models. The resulting method allows a very stable simulation of arbitrary three-dimensional structures avoiding the formation of unphysical surface loops which result from a moving surface intersecting with itself. The cellular material representation allows efficient shadow and visibility computation which are needed to calculate the particle flux of directly and indirectly incident particles.

References

[1] K. K. H. Toh, A. R. Neureuther, and E. W. Scheckler, "Algorithms for simulation of three-dimensional etching," *IEEE Trans. Computer-Aided Design,* vol. 13, pp. 616–624, May 1994.

[2] E. W. Scheckler, N. N. Tam, A. K. Pfau, and A. R. Neureuther, "An efficient volume-removal algorithm for practical three-dimensional lithography simulation with experimental verification," *IEEE Trans. Computer-Aided Design,* vol. 12, pp. 1345–1356, Sept. 1993.

[3] W. Henke, D. Mewes, M. Weiss, G. Czech, and R. Schliessl-Hoyler, "A study of reticle defects imaged into three-dimensional developed profiles of positive photoresists using the SOLID lithography simulator," *Microelectron. Eng.,* vol. 14, pp. 283–297, Nov. 1991.

[4] Y. Hirai, S. Tomida, K. Ikeda, M. Sasago, M. Endo, S. Hayama, and N. Nomura, "Three-dimensional resist process simulator PEACE (Photo and Electron Beam Lithography Analyzing Computer Engineering System," *IEEE Trans. Computer-Aided Design,* vol. 10, pp. 802–807, June 1991.

[5] T. Ishizuka, "Bulk image effects of photoresist in three-dimensional profile simulation," *J. Computation Math. Elect. Electron. Eng.,* vol. 10, no. 4, pp. 389–399, 1991.

[6] A. Moniwa, T. Matsuzawa, T. Ito, and H. Sunami, "Three-dimensional photoresist imaging process simulator for strong standing-wave effect environment," *IEEE Trans. Computer-Aided Design,* vol. CAD-6, pp. 431–437, May 1987.

[7] F. Jones and J. Paraszczak, "RD3D (Computer simulation of resist development in three dimensions)," *IEEE Trans. Electron Devices,* vol. ED-28, pp. 1544–1552, Dec. 1981.

[8] E. W. Scheckler and A. R. Neureuther, "Models and algorithms for three-dimensional topography simulation with SAMPLE-3D," *IEEE Trans. Computer-Aided Design,* vol. 13, pp. 219–230, Feb. 1994.

[9] J. Pelka, "Three-dimensional simulation of ion-enhanced dry-etch processes," *Microelectron. Eng.,* vol. 14, no. 3–4, pp. 269–281, 1991.

[10] S. Tazawa, F. A. Leon, G. D. Anderson, T. Abe, K. Saito, A. Yoshii, and D. L. Scharfetter, "3-D topography simulation of via holes using generalized solid modeling," in *Proc. Int. Electron Devices Meeting,* 1992, pp. 173–176.

[11] M. Fujinaga, N. Kotani, T. Kunikiyo, H. Oda, M. Shirahata, and Y. Akasaka, "Three-dimensional topography simulation model: etching and lithography," *IEEE Trans. Electron Devices,* vol. 37, pp. 2183–2192, Oct. 1990.

[12] K. K. H. Toh, "Algorithms for three-dimensional simulation of photoresist development," Ph.D. dissertation, EECS Dept., Univ. of California, Berkeley, 1990.

[13] J. J. Helmsen, E. W. Scheckler, A. R. Neureuther, and C. H. Séquin, "An efficient loop detection and removal algorithm for 3D surface-based lithography simulation," in *Proc. Workshop Numerical Modeling Processes Devices Integrated Circuits,* 1992, pp. 3–8.

[14] C. R. Giardina and E. R. Dougherty, *Morphological Methods in Image and Signal Processing.* Englewood Cliffs, NJ: Prentice-Hall, 1988.

[15] E. Strasser, K. Wimmer, and S. Selberherr, "A new method for simulation of etching and deposition processes," in *Proc. 1993 Int. Workshop VLSI Process Device Modeling,* 1993, pp. 54–55.

[16] E. Strasser, G. Schrom, K. Wimmer, and S. Selberherr, "Accurate simulation of pattern transfer processes using Minkowski operations," *IEICE Trans. Electron.,* vol. E77-C, pp. 92–97, Feb. 1994.

[17] W. G. Oldham, A. R. Neureuther, C. Sung, J. L. Reynolds, and S. N. Nandgaonkar, "A general simulator for VLSI lithography and etching processes: Part II—Application to deposition and etching," *IEEE Trans. Electron Devices,* vol. ED-27, pp. 1455–1459, Aug. 1980.

[18] J. Lorenz, J. Pelka, H. Ryssel, A. Sachs, A. Seidel, and M. Svoboda, "COMPOSITE—A complete modeling program of silicon technology," *IEEE Trans. Computer-Aided Design,* vol. CAD-4, pp. 421–430, Oct. 1985.

[19] S. Tazawa, S. Matsuo, and K. Saito, "Unified topography simulator for complex reaction including both deposition and etching," in *Proc. 1989 Symp. VLSI Technol.,* 1989, pp. 45–46.

[20] J. P. McVittie, J. C. Rey, L. Y. Cheng, A. Bariya, S. Ravi, and K. Saraswat, "SPEEDIE: A profile simulator for etching and deposition," in *Proc. TECHNOCON,* 1990, pp. 16–19.

[21] S. Tazawa, S. Matsuo, and K. Saito, "A general charakterization and simulation method for deposition and etching technology," *IEEE Trans. Semiconductor Manufacturing,* vol. 5, pp. 27–33, Feb. 1992.

[22] E. W. Scheckler, K. K. H. Toh, D. M. Hoffstetter, and A. R. Neureuther, "3D lithography, etching, and deposition simulation (SAMPLE-3D)," in *Proc. 1991 Symp. VLSI Technol.,* 1991, pp. 97–98.

[23] I. A. Blech, "Evaporated film profiles over steps in substrates," *Thin Solid Films,* vol. 6, pp. 113–118, 1970.

[24] Y. Eguchi, M. IslamRaja, J. P. McVittie, and K. Saraswat, "Profile modeling of physical vapor deposition of Ti and WSi_x," in *Proc. Symp. Process Physics Modeling Semiconductor Technol.,* 1993, pp. 301–309.

[25] E. W. Scheckler, "Algorithms for three-dimensional simulation of etching and deposition processes in integrated circuit fabrication," Ph.D. dissertation, EECS Dept., Univ. of California, Berkeley, 1991.

[26] D. Temmler, "Multilayer vertical stacked capacitors (MVSTC) for 64 Mbit and 256 Mbit DRAM's," in *Proc. 1991 Symp. VLSI Technol.,* 1991, pp. 13–14.

Ernst Strasser (S'93) was born in Salzburg, Austria, in 1966. He studied electrical engineering at the Technical University of Vienna, where he received the Diplomingenieur degree in 1991. In December 1994, he received the doctoral degree from the same university.

In January 1992, he joined the Institut für Mikroelektronik working on three-dimensional topography simulation. His current work is focused on algorithms and mathematical models for three-dimensional process simulation in integrated circuit fabrication.

Siegfried Selberherr (M'79–SM'84–F'93) was born in 1955. He received the Diplomingenieur degree in control theory and industrial electronics from the Technical University of Vienna in 1978. He finished the doctorate degree on "Two dimensional MOS-transistor modeling" in 1981.

After receiving the Diplomingenieur degree, he joined the Technical University of Vienna as Researcher. Since 1984, he has been holding the "venia docendi" on Computer-Aided Design as a Professor. He is the head of the Institut für Mikroelektronik since 1988. In 1994, he was appointed head of the Computing Services Center of the Technical University of Vienna. His current research topics are modeling and simulation of problems for microelectronics engineering.

Dr. Selberherr has authored and coauthored more than 250 publications in journals and conference proceedings. Furthermore, he wrote a book *Analysis and Simulation of Semiconductor Devices.* In 1983, he received the Dr. Ernst Fehrer award; in 1985 he received the award of the Nachrichtentechnische Gesellschaft; in 1986 he was honored with the Dr. Herta Firnberg Staatspreis; and in 1987 he received the Heinz Zemanek award. In 1993, he was elected Fellow of the IEEE "for pioneering work in numerical analysis of semiconductor devices and their processes." In 1994, he was honored with the Wilhelm-Exner-Medal. He is a member of the Association for Computing Machinery (1979), the Society of Industrial and Applied Mathematics (1980), and the Verband deutscher Elektrotechniker (1984). He is Editor of *The Transactions of the Society for Computer Simulation* (1983–), *Electrosoft* (1986–1991), *Mikroelektronik* (1988–), and of the Springer-Verlag book series *Computational Microelectronics* (1985–). He serves on the Programme Advisory Board of *Electron Technology* (1994–).